Imaging of magnetic vortices in superconducting networks and clusters by scanning SQUID microscopy

L. N. Vu, M. S. Wistrom, and D. J. Van Harlingen
Department of Physics, University of Illinois at Urbana-Champaign, 1110 W. Green Street, Urbana, Illinois 61801

(Received 7 June 1993; accepted for publication 26 July 1993)

We have imaged the configuration of trapped magnetic vortices in two-dimensional superconductor arrays and clusters using a scanning SQUID microscope (SSM). The SSM scans a dc SQUID detector over the array surface, achieving better than 10 μm spatial resolution over a scan range up to 1 cm$\times$1 cm and a magnetic flux sensitivity of about $10^{-4}\Phi_0$. We have obtained images of large square arrays cooled at different values of applied magnetic flux per cell Φ. For low rational values ($\frac{1}{2},\frac{1}{3},\frac{1}{4},\ldots$) of the frustration parameter $f=\Phi/\Phi_0$, we find regions of periodically arranged vortices separated by domain walls; at other values of the field, the vortex pattern is disordered. We also present observations of vortex patterns in ensembles of 3$\times$3 clusters.

Arrays of Josephson tunnel junctions and networks of superconducting lines have attracted much scientific interest because they are isomorphic to a uniformly frustrated XY model in an applied magnetic field, exhibit two-dimensional topological phase transitions, and can be used to model phase coherence and vortex dynamics relevant to granular superconducting films and high-T_c superconducting films.[1] Much of the theoretical work has concentrated on calculations of the ground state configurations of vortices and their corresponding free energies for arrays in a magnetic field.[2,3] Until recently, however, it has not been possible to observe vortices in arrays because the magnetic fields associated with them are very weak. Instead, experiments have measured the electronic transport properties which are related to the averaged vortex dynamics of the arrays near the transition temperature.[4,5] Direct detection of vortex configurations and motion has been a long-standing experimental goal and offers an exciting path toward understanding phase coherence, frustration, commensurability, and vortex dynamics and interactions in superconductor arrays and networks.

In this letter, we report the imaging of magnetic vortex configurations for different applied magnetic fields in square networks of Nb lines with cell sizes of 20 μm$\times$20 μm. To do this, we have developed an instrument we call the scanning SQUID microscope (SSM). In this instrument, a sensitive dc SQUID detector is scanned in two dimensions over the array surface to map out the magnetic field modulations due to the trapped vortices. The SSM offers substantially higher flux sensitivity and a larger scan range than scanning Hall probes[6] that have been used to image vortices in superconducting networks with small cell areas, or magnetic force microscopy,[7] which is trying to be developed for this purpose. In addition, the SSM is able to detect not only the vortices but also the geometry of the underlying superconductor lattice, allowing determination of the commensurability of the vortex pattern. Scanning techniques using SQUIDs have been previously used to measure field variations at higher temperature and on a larger spatial scale.[8]

The design of the SSM has been described previously.[9] Figure 1(a) shows the sealed sample chamber that houses the SQUID and the array sample; both are cooled via helium exchange gas by a liquid helium reservoir located above the chamber. The sample is mounted on top of a copper block at the end of a rigid, low thermal conductance shaft connected to a room-temperature x-y-z manipulator. The temperature of the sample is monitored with a Ge diode thermometer and varied by injecting current into a resistor imbedded in the copper block. The sample chamber is isolated from the system vacuum jacket by a soft welded stainless-steel bellows that shears as the sample shaft is scanned. The x-y motion of the sample is driven by computer-controlled stepping motors and has a scan range up to 1 cm with a spatial resolution of 2 μm. The z position can be adjusted manually with comparable resolution.

A dc SQUID operated in a flux-locked mode detects the vertical component of the field at the surface of the sample. The spatial resolution is determined by the size of the SQUID loop and its distance above the surface of the array. For the measurements reported here, we used a Nb-trilayer dc SQUID with a loop size of 10 μm$\times$10 μm fabricated within 50 μm of the edge of a sapphire substrate, as shown in Fig. 1(b). The tunnel junctions have areas of 2 μm^2 and are separated from the SQUID loop by long, parallel leads to minimize screening of the applied magnetic flux through the array by the superconducting films. The leads are shielded with a superconducting ground plane so that most of the pickup is in the loop. The SQUID is mounted on a flexible Mylar hinge above the array so that the tip of substrate near the SQUID rests lightly by gravity against the sample surface. By varying z, we can adjust the angle between the sample and detector substrate to a few degrees, placing the SQUID within about 5 μm of the array. The SQUID follows the contour of the sample surface during scanning. A Helmholtz coil provides a uniform magnetic field as the array is cooled through its transition temperature. The SQUID and array are shielded by a superconducting Pb can inside the sample chamber and a single layer of μ-metal around the outside of the SSM.

In operation, the SSM achieves spatial resolution of better than 10 μm and a scan range of 1 cm$\times$1 cm. A

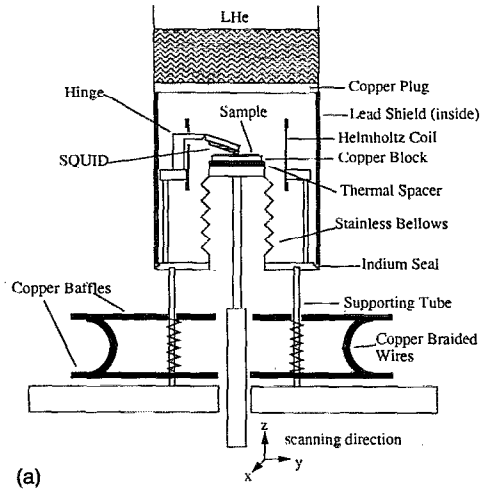

(a)

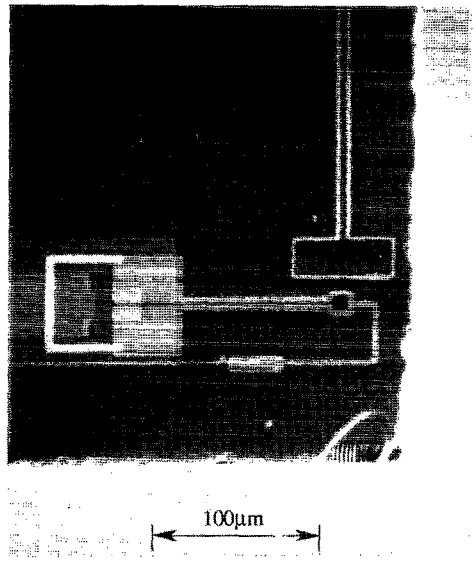

(b)

FIG. 1. (a) The design of the SSM, showing the scanning mechanism and the hinge assembly used to maintain close proximity of the SQUID to the array. (b) An electron micrograph of the dc SQUID chip.

typical scan of 128×128 pixels over an area of 500 μm $\times500$ μm takes about 30 min to acquire, limited by the speed and acceleration of the stepping motors. At this rate, the flux signal is averaged at each pixel for 0.1 s. Since the bare dc SQUID noise is about $3\times10^{-6}\Phi_0/\mathrm{Hz}^{1/2}$, the expected magnetic flux sensitivity is about $10^{-5}\Phi_0$. In practice, vibration and electromagnetic interference from the stepping motors degrade the ultimate sensitivity by an order of magnitude but has not been found to affect the locking of the SQUID feedback loop.

To demonstrate the performance and capability of the SSM, we have imaged the configurations of vortices trapped in Nb wire networks. The networks consist of sputtered Nb lines of width 2 μm and thickness 120 nm. The cell size is 20 μm$\times$20 μm. A 500 nm layer of SiO is evaporated on top of the array to protect the pattern during scanning. In our measurements, we apply a uniform magnetic field above the Nb transition temperature (9 K) and cool the sample into its superconducting state. The

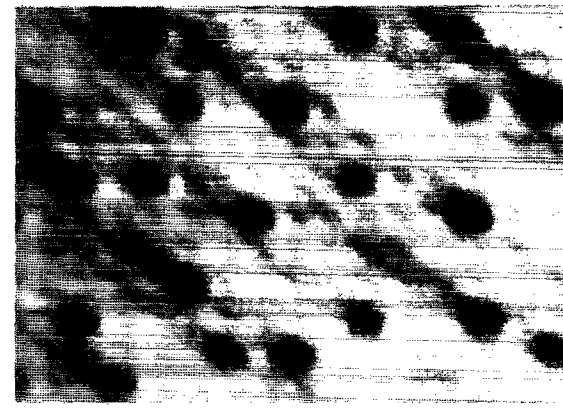

FIG. 2. A magnetic flux image of a square Nb wire network cooled near zero field, showing a few trapped vortices and the pattern of the underlying superconducting lines. The cell size is 20 μm$\times$20 μm.

important parameter is the frustration $f=\Phi/\Phi_0$, the applied magnetic flux per cell.

Figure 2 shows a vortex image of a section of a Nb network cooled in zero applied magnetic field. The black dots show the location of trapped vortices in the array. From the observed vortex density $\sim0.03\Phi_0$/cell, we estimate that there is a residual magnetic field of about 5 mG in the sample chamber. The diagonal streaks in these images are due to a small pickup of magnetic field in the connections leading to the SQUID loop [see Fig. 1(b)], which is oriented at 45° with respect to the scan direction. Besides the vortices, the grid of superconducting lines is also directly observable. This occurs because the SQUID loop is partially screened by the superconducting Nb as it passes over the line, causing a shift in the dc feedback flux to the SQUID loop. By adjusting the height of the SQUID above the sample and the dc flux bias point of the SQUID, the contrast between the grid and the trapped vortex fields can be adjusted, making it either very sharp or tuning it out. Seeing the underlying grids is particularly advantageous for imaging finite size samples and complex, nonperiodic networks.

In Fig. 3, we present a series of vortex images attained at low rational values of flux $f=\frac{1}{5}$, $\frac{1}{4}$, $\frac{1}{3}$, and $\frac{1}{2}$. Next to the image, we show the predicted ground state vortex pattern at that flux. At $f=\frac{1}{2}$, the vortices are expected to arrange in a checkerboard pattern, occupying every other cell. This is observed over areas of typically 10×10 cells, but we also find domain walls separating regions of opposite chirality. Such domain walls have excitation energies comparable to vortex-antivortex pairs and may be important in the transport properties of arrays near $f=\frac{1}{2}$. At $f=\frac{1}{3}$, the ground state is expected to be a series of diagonal rows of vortices. There are six degenerate ground state configurations of this type, and we observe orthogonal rows of vortices as the configurations compete. Our images at $f=\frac{1}{5}$ also agree reasonably well with the predicted vortex pattern but with more disorder. At $f=\frac{1}{4}$, the disorder is substantially greater and it is difficult to identify regions in the image that correspond to the calculated pattern. At this field, the

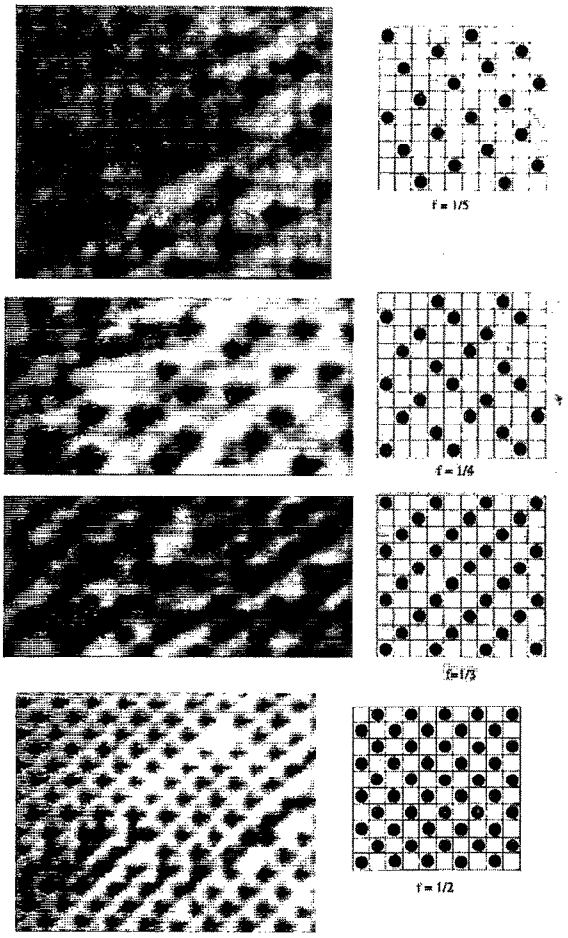

FIG. 3. Vortex images of networks cooled at fields corresponding to magnetic flux per cell $f=\Phi/\Phi_0=\frac{1}{5}, \frac{1}{4}, \frac{1}{3}$, and $\frac{1}{2}$. Adjacent to each image we show the configuration of vortices calculated to have the lowest energy at each field.

energy of the ground state vortex pattern is only slightly lower than alternate metastable configurations so that variations in the cluster geometry and thermal fluctuations cause significant disorder. Note that at this field the vortices are not expected to align in rows as is expected at the other fields studied. For arrays cooled at fields for which f is not a low rational value, the observed vortex pattern is random. In arrays cooled near zero field, we also occasionally detect vortex–antivortex pairs in the network, corresponding to opposite polarity vortices in adjacent cells.

Finally, in Fig. 4, we show vortex images for an ensemble of 3×3 clusters at two different magnetic fields. At $f=0.2$ each cluster can either capture the 1 or 0 vortex, with a single vortex in the center cell being the lowest energy state and therefore the most probable. At $f=0.6$, the situation is more complicated with many different possible configurations containing 4, 5, 6, and 7 trapped vortices observed. At this field, the energies of these different states are closely spaced so that thermal fluctuations during the cooling process can activate the cluster into one of many possible configurations. Using computer simulations of the vortex dynamics in the clusters, it is possible to calculate the free energy curves for each vortex configuration and then calculate statistics for an ensemble of clusters. Comparison of this modeling with the observed statistical distributions gives information on the extent of coupling disorder in the clusters[10] and the thermodynamics of the flux trapping process.[11]

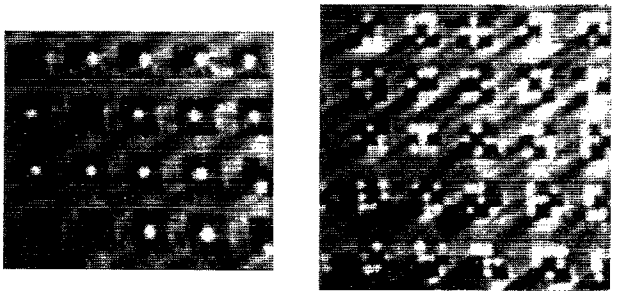

FIG. 4. Vortex configurations in an ensemble of 3×3 clusters cooled in fields corresponding to a flux per cell of (a) $f=0.2$ and (b) $f=0.6$. The relative probability of each pattern depends on the configuration energy when the vortices become trapped during quenching.

In conclusion, we have developed a scanning SQUID microscope that is capable of imaging vortex configurations in microfabricated superconductor arrays and clusters. We have demonstrated the sensitivity, spatial resolution, and range of this instrument by studying static vortex distributions in large square arrays and 3×3 clusters. Direct imaging of vortices opens up unlimited opportunities for investigating interactions of vortices with the underlying lattice, defects, and each other and complement experimental work that has probed the dynamics of vortices in these systems.

We thank Matt Hauser and Joe Walko for the development of image acquisition software, and Subashri Rao and Fang Yu for useful discussions. This work is supported by the National Science Foundation under Grant NSF-DMR 91-15411. We acknowledge extensive use of thin film microfabrication facilities of the Frederick Seitz Materials Research Laboratory at the University of Illinois.

[1] For a review of this field, see J. E. Mooij and G. Schön, Physica B **152** (1988).
[2] S. Teitel and C. Jayaprakash, Phys. Rev. Lett. **51**, 1999 (1983); Phys. Rev. B **27**, 598 (1983).
[3] T. C. Halsey, Phys. Rev. Lett. **55**, 1018 (1985); Phys. Rev. B **31**, 5728 (1985).
[4] See, for example, R. F. Voss and R. A. Webb, Phys. Rev. B **25**, 3446 (1982); D. W. Abraham, C. J. Lobb, M. Tinkham, and T. J. Klapwijk, Phys. Rev. B **26**, 5268 (1982); K. N. Springer and D. J. Van Harlingen, Phys. Rev. B **36**, 7273 (1987).
[5] C. J. Lobb, D. W. Abraham, and M. Tinkham, Phys. Rev. B. **27**, 1150 (1983).
[6] A. M. Chang, H. D. Hallen, L. Harriott, H. F. Hess, H. L. Kao, J. Kwo, R. E. Miller, R. Wolfe, J. van der Ziel, and T. Y. Chang, Appl. Phys. Lett. **61**, 1974 (1992).
[7] Y. Martin, D. Rugar, and H. K. Wickramasinghe, Appl. Phys. Lett. **52**, 244 (1988).
[8] R. C. Black, A. Mathai, F. C. Wellstood, E. Danister, A. II. Miklich, D. T. Nemeth, J. J. Kingston, and J. Clarke, Appl. Phys. Lett. **62**, 2128 (1993).
[9] L. N. Vu and D. J. Van Harlingen, IEEE Trans. Appl. Superconduct. **3**, 1918 (1993).
[10] S. V. Rao and D. J. Van Harlingen, Phys. Rev. B (to be published).
[11] L. N. Vu, S. V. Rao, and D. J. Van Harlingen (unpublished).